**Turkish Computational and Theoretical Chemistry**

*Turkish Comp Theo Chem (TC&TC)*

***Volume(Issue): 5(1) – Year: 2021 – Pages: 27-38***

***e-ISSN: 2602-3237***

***https://doi.org/10.33435/tcandtc.843329***

***Received:*** 19.12.2020 ***Accepted:*** 22.02.2021 *Research Article*

# *2-Acetyl-5-chloro-thiophene thiosemicarbazone and its nickel(II) and zinc(II) complexes: Hirshfeld surface analysis and Density Functional Theory calculations for molecular geometry, vibrational spectra and HOMO-LUMO studies*

**Betül ŞEN YÜKSEL** [1,a]

[a] Dokuz Eylül University, Department of Physics, 35390, Buca, Izmir, Turkey

**Abstract:** In this work, the theoretical studies on the molecular structure are presented for 2-Acetyl-5-chloro-thiophene thiosemicarbazone and its Ni(II) and Zn(II) complexes. The optimized molecular geometry and fundamental vibrational frequency values have been investigated with the help of DFT/B3LYP method using 6-31G(d,p) basis set and they are found to be in agreement with the experimental values. Additionally, frontier molecular orbital energies (HOMO, LUMO) and their energy gaps (ΔE) are calculated by the same method. The HOMO and LUMO analysis are used to determine some molecular properties such as chemical potential, hardness, softness and electronegativity. Furthermore, Hirshfeld surface analyses and fingerprint plots have been used for visualizing and exploring intermolecular interactions in the crystal structure and for determining the percentage contribution of these interactions on the surface. The Hirshfeld surface analysis and the 2D fingerprint plots indicate that the crystal packing of the compounds is dominated by Cl···H/H···Cl, S···H/ H···S, N···H/ H···N and H···H contacts.

***Keywords:*** *Thiosemicarbazones, DFT calculations, Hirshfeld surface analysis.*

## 1. Introduction

Thiosemicarbazones are versatile ligands, including appropriate donor atoms for coordination to metals [1,2]. They have tautomerism such as thione or thiol tautomer, and the ability to coordinate to metal ions either in neutral or anionic form, acting usually as monodentate or bidentate ligands depending on whether the bonding takes place via azomethine nitrogen and thio-carbonyl sulfur atoms [3,4]. Thiosemicarbazones, as well as their transition metal complexes, possess a wide variety of pharmacological activity inclusive of antifungal [5,6], antitumor [7,8], antibacterial [9,10], anti-malarial [11,12], antiviral [13] and anti-cancer [14,15]. Particularly, transition metals such as Co(II), Ni(II), Cu(II), Zn(II) and Pd(II) coordinated to thiosemicarbazone ligands attract a great deal of interest due to their chemical behavior and biological activity [16]. In addition, metal complexes have been extensively used for device applications in telecommunications, optical computing, optical storage and optical information processing [17].

As seen from the above discussions, these metal complexes are important not only in academic grounds but also they can be treated as potential candidates in technological and medical applications. Therefore, in recent years, we have been working on the structural and biological properties of thiosemicarbazones and their metal complexes. The aim of this study is to give a complete description of the molecular geometry, molecular vibrations and HOMO–LUMO energies of ligand and its two complexes. We also report herein investigation of intermolecular contacts by Hirshfeld surface analysis. Furthermore, the results of calculations obtained by density functional theory (DFT) B3LYP with 6-31G(d,p) level are compared with the experimentally determined

[1] Corresponding Authors

e-mail: betul.sen@deu.edu.tr

molecular structure and also with the spectroscopic results.

## 2. Method

### 2.1. Synthesis of ligand and its complexes

The 2-Acetyl-5-chloro-thiophene thiosemicarbazone was synthesized according to the method described in the literature [18] while complexes were prepared from 2-Acetyl-5-chloro-thiophene thiosemicarbazone by the literature procedure [15].

### 2.2. Crystal structures of ligand and its complexes

The crystal structures of the ligand and complexes were determined by the X-ray diffraction method in previous studies [15,18].

### 2.3. Computational details

Density functional theory calculations using the Becke's three parameter hybrid functional were performed using Lee-Yang-Parr correlation functional implemented with 6-31G(d,p) [19-21]. The geometrical parameters, frontier molecular orbital energies and vibrational frequency (FT-IR) calculations were carried out by using the Gaussian 09W program package [22]. The structure of the optimized geometry and pictures of HOMO-LUMO energies were constructed by GaussView 5.0 [23] program. The structures obtained from the optimized geometry of all compounds were stable structures due to the absence of imaginary frequencies in the calculated IR spectrum.

### 2.4. Hirshfeld surfaces computational method

The determination of Hirshfeld surface (HS) and analysis of the corresponding fingerprint plot (FP) provide us an efficient and reasonably effective method for the aims of the visualization and comparison of various intermolecular interactions present within a crystal structure. The fingerprint plot represents the two-dimensional (di, de) contacts, where di indicates the distance from a point on the surface to the nearest nucleus inside the surface and de indicates the distance of the nearest nucleus outside the surface on HS. The normalized contact distance dnorm, is based on both di and de, each of which is normalized by the van der Waals radii of their corresponding atoms involved in the close contact to the surface. The value of dnorm is negative when intermolecular contacts are shorter than the sum of the van der Waals radii of the two atoms, which is visualized as red spots in the Hirshfeld surface. The white color denotes the contacts with distances close to the sum of the van der Waals radii corresponding to dnorm value of zero while contacts longer than the sum of van der Waals radii resulting in positive dnorm value are highlighted in blue color on the surface. The three-dimensional HSs [24] mapped to dnorm and their associated two-dimensional FPs analysis, as well as shape-index and curvedness presented in this study were generated for all compounds based upon the crystallographic information file (CIF) using CrystalExplorer 3.1 [25].

## 3. Results and discussion

### 3.1. Molecular geometry

For the theoretical investigation of structures, the starting geometry was obtained from the X-ray structure determination, and the molecular geometry was optimized using DFT in the ground state. The optimized geometric structures of all compounds are shown in Figure 1. Some optimized parameters such as bond lengths and bond angles are given in Table 1 and compared with the experimental data.

The root mean square error (RMSE) reported by Palafox [26] is used for a comparison of theoretical and experimental values for geometric parameters. The RMSE is separately calculated for geometric parameters, namely the bond length and the bond angle for each complex.

The RMSE values are obtained as 0.023 Å (ligand), 0.027 Å (Zn-complex) and 0.024 Å (Ni-complex) for bond length whereas they are found as 1.30 Å (ligand), 2.32 Å (Zn-complex) and 1.37 Å (Ni-complex) for bond angle. Zn-complex has the largest deviation in bond angles between experimental and calculated values due to the mismatch of bond angles around metal atom. Coordination environment bond angles which have the greatest difference between experimental and theoretical values are observed as 117.90 and 113.21o for S1–Zn1–S1i and Cl2–Zn1–Cl2i whereas they are calculated as112.20 and 120.60.
Note that the reason for general deviation in results is that the intra- and intermolecular forces present

in the solid state are taken into account in the X-ray study whereas these forces are not considered in the calculations.

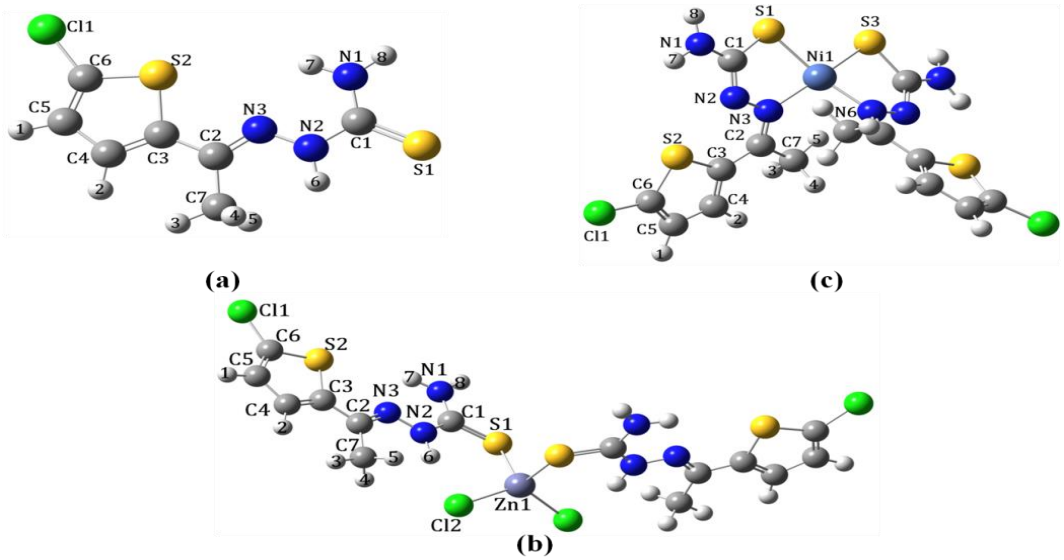


**Figure 1.** The optimized structures of (a) Ligand, (b) Zn-complex and (c) Ni-complex

### 3.2. HOMO-LUMO Analysis

Frontier molecular orbitals (FMOs) analysis plays an important role in determining molecular electrical transport properties and molecular stability. LUMO (the lowest unoccupied molecular orbital) acts as an electron acceptor representing the ability to obtain an electron while HOMO (highest occupied molecular orbital) is regarded as an electron donor representing the ability to donate an electron. According to Figures 2a-b, the LUMO of ligand and Zn-complex is mainly located on the 5-chloro thiophene rings. Besides, the HOMO is found to be localized around the whole molecule except the methyl group for ligand while it is distributed over the whole molecule except the methyl group, Zn and Cl atoms for Zn-complex. The orbital diagrams of Ni-complex in Figure 2c indicate that HOMO is located over the whole of the molecule except the methyl groups and 5-chloro thiophene rings whereas LUMO is spread over the entire molecule except CH3 group, Ni atom and S atoms bonded to Ni atom. The distributions and energy levels of the HOMO and LUMO orbitals are calculated at the B3LYP level for compounds. Some quantities related to energies such as the chemical hardness (η=(ELUMO-EHOMO)/2), chemical softness (S=1/2η) and the electronegativity (□=-(ELUMO+EHOMO)/2) are also computed from LUMO and HOMO energy values. The HOMO-LUMO energy gap (ΔE) is an important stability parameter indicating the chemical stability of the molecule. The molecular orbital energy gap for the ligand is 3.691 eV which can be compared with those obtained for Zn-complex (3.966 eV) and Ni-complex (3.363 eV). According to Table 2, we can conclude that the large energy gap, highest hardness and lowest softness indicate that Zn-complex is more stable and less reactive than ligand and Ni-complex.

### 3.3. Vibrational spectra

Calculated harmonic vibrational frequencies may be usually found to be greater than those obtained for the corresponding experimental values due to the lack of properly inclusion of the electron correlation effects and basis sets deficiencies in the calculations [27]. In this regard, by using a proper scale factor, it may be possible to obtain theoretical results that are in agreement with the experimental values. In the present study, the calculated harmonic frequencies are scaled down using a single scaling factor 0.9608 for B3LYP/6-31G (d,p) [28]. Selected calculated vibrational frequencies of the compounds and their assignments are shown in Table 3.

RMSE values are found to be 14.74, 20.09 and 19.40 cm-1, respectively for ligand, Zn- and Ni-complexes. These results indicate that the

frequencies calculated for compounds show good agreement with experimental values.

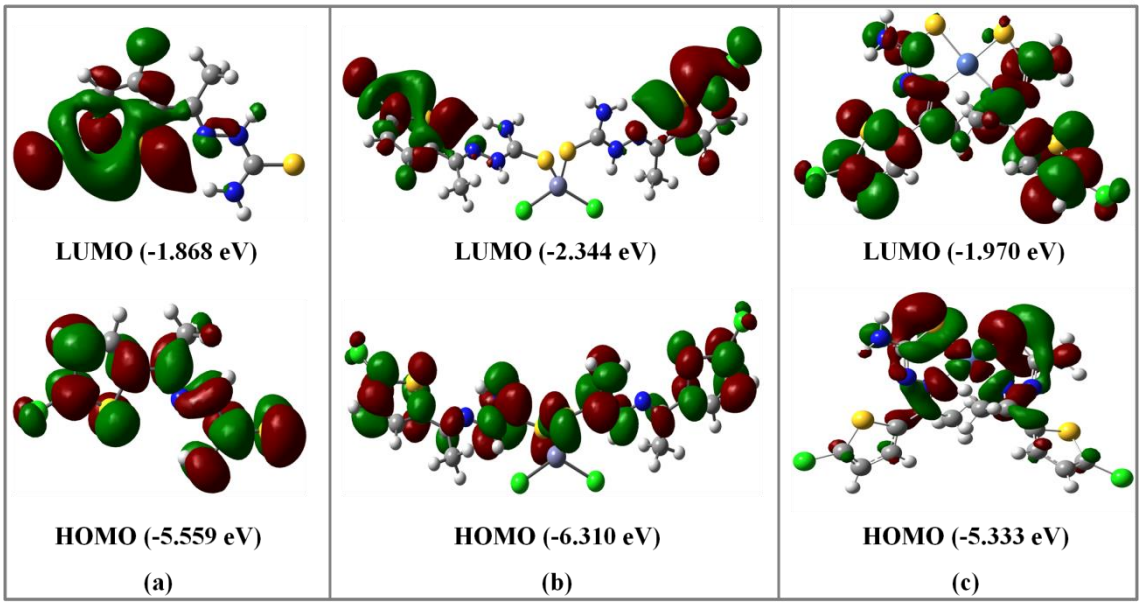


**Figure 2.** Molecular orbital surfaces and energy levels for the LUMO and HOMO of (a) Ligand, (b) Zn-complex and (c) Ni-complex.

**Table 1.** Selected optimized geometrical parameters of Ligand, Zn- and Ni-complexes.

| Parameters | Ligand | Parameters | Zn-complex | Parameters | Ni-complex |
|---|---|---|---|---|---|
| *Bond lengths (Å)* | | | | | |
| Cl1–C6 | 1.730 | Cl1–C6 | 1.729 | Cl1–C6 | 1.733 |
| S1–C1 | 1.678 | S1–C1 | 1.717 | S1–C1 | 1.755 |
| S2–C6 | 1.743 | S2–C6 | 1.742 | S2–C6 | 1.742 |
| S2–C3 | 1.758 | S2–C3 | 1.758 | S2–C3 | 1.764 |
| N1–C1 | 1.344 | N1–C1 | 1.338 | N1–C1 | 1.355 |
| N2–N3 | 1.355 | N2–N3 | 1.370 | N2–N3 | 1.381 |
| N2–C1 | 1.376 | N2–C1 | 1.352 | N2–C1 | 1.314 |
| N3–C2 | 1.298 | N3–C2 | 1.296 | N3–C2 | 1.312 |
| C2–C3 | 1.456 | C2–C3 | 1.458 | C2–C3 | 1.452 |
| C2–C7 | 1.510 | C2–C7 | 1.506 | C2–C7 | 1.508 |
| C3–C4 | 1.378 | C3–C4 | 1.378 | C3–C4 | 1.387 |
| C4–C5 | 1.423 | C4–C5 | 1.422 | C4–C5 | 1.415 |
| C5–C6 | 1.367 | C5–C6 | 1.368 | C5–C6 | 1.370 |
| | | Zn1–S1 | 2.434 | Ni–S1 | 2.199 |
| | | Zn1–Cl2 | 2.261 | Ni–N3 | 1.905 |
| **RMSE*** | 0.023 | | 0.027 | | 0.024 |
| *Bond angles (°)* | | | | | |
| C6–S2–C3 | 90.71 | C6–S2–C3 | 90.70 | C6–S2–C3 | 90.46 |
| C1–N2–N3 | 121.36 | C1–N2–N3 | 117.86 | C1–N2–N3 | 112.30 |
| C2–N3–N2 | 119.06 | C2–N3–N2 | 119.55 | C2–N3–N2 | 115.36 |
| N1–C1–S1 | 125.11 | N1–C1–S1 | 119.48 | N1–C1–S1 | 118.33 |
| N1–C1–N2 | 115.13 | N1–C1–N2 | 117.00 | N1–C1–N2 | 118.21 |
| N2–C1–S1 | 119.76 | N2–C1–S1 | 123.50 | N2–C1–S1 | 123.38 |
| N3–C2–C3 | 116.54 | N3–C2–C3 | 115.48 | N3–C2–C3 | 124.26 |

| | | | | | |
|---|---|---|---|---|---|
| N3–C2–C7 | 123.23 | N3–C2–C7 | 124.57 | N3–C2–C7 | 118.74 |
| C3–C2–C7 | 120.23 | C3–C2–C7 | 119.95 | C3–C2–C7 | 116.97 |
| C2–C3–S2 | 119.92 | C2–C3–S2 | 120.06 | C2–C3–S2 | 125.28 |
| C4–C3–S2 | 110.60 | C4–C3–S2 | 110.61 | C4–C3–S2 | 110.16 |
| C4–C3–C2 | 129.48 | C4–C3–C2 | 129.34 | C4–C3–C2 | 124.55 |
| C3–C4–C5 | 114.03 | C3–C4–C5 | 114.04 | C3–C4–C5 | 114.61 |
| C6–C5–C4 | 111.76 | C6–C5–C4 | 111.74 | C6–C5–C4 | 111.23 |
| S2–C6–Cl1 | 120.36 | S2–C6–Cl1 | 120.41 | S2–C6–Cl1 | 120.32 |
| C5–C6–Cl1 | 126.75 | C5–C6–Cl1 | 126.67 | C5–C6–Cl1 | 126.15 |
| C5–C6–S2 | 112.89 | C5–C6–S2 | 112.92 | C5–C6–S2 | 113.53 |
| | | S1–Zn1–S1$^{i}$ | 113.21 | S3–Ni1–S1 | 95.19 |
| | | S1–Zn1–Cl2 | 108.41 | N3–Ni1–S1 | 86.11 |
| | | S1–Zn1–Cl2$^{i}$ | 103.0 | N3–Ni1–S3 | 160.52 |
| | | Cl2–Zn1–Cl2$^{i}$ | 120.60 | N3–Ni1–N6 | 99.02 |
| | | | | N6–Ni1–S1 | 160.72 |
| | | | | N6–Ni1–S3 | 86.14 |
| **RMSE*** | 1.30 | | 2.32 | | 1.37 |

*Experimental values for the calculation of RMSE are used from Ref. [18] for ligand and from Ref. [15] for Zn- and Ni-complexes. Symmetry code: (i)1-x,+y,3/2-z

N–H vibrations

The high frequency area in the left part of the FT-IR spectrum above 3000 cm-1 appears as a characteristic region representing N–H stretching vibrations [29]. The values of the NH2 symmetric stretching vibrations obtained from B3LYP method are found at 3244.4 cm-1 (ligand), 3274.0 cm-1 (Zn-complex) and 3358.8 cm-1 (Ni-complex) while these frequencies are observed in the experimental spectrum at 3223, 3296 and 3384 cm-1,respectively. The bands at 3151 and 3157 cm-1 belong to hydrazine νNH vibration in the experimental spectra of the ligand and Zn-complex, respectively, whereas vibrations obtained from B3LYP method corresponding to those are found at 3167.3 and 3131.0 cm-1. This band is absent from IR and theoretical spectrum of Ni-complex indicating that the ligand in complex emerges as the thiol tautomer in the solid-state when passing from the ligand to complex.

C=N vibrations

The observed shift towards higher or lower frequency in C=N bands during complexation indicates the evidence of coordination of metal atom with an azomethine nitrogen atom. After the complexation, the C=N bond stretching vibrations of Ni-complex are experimentally observed at 1547 cm-1 which exhibits a shift to a lower frequency region in comparison with the free ligand counterparts [1575 cm-1] by about 28 cm-1. This observation points out that, as also reported in the previous X-ray studies, thiosemicarbazones are coordinated to the metal center as a bidentate ligand through azomethine nitrogen and thiocarbonyl sulphur atoms. The C=N vibrations of Zn-complex that appeared at 1573 cm-1 are almost the same in comparison with those observed for the ligand. These stretching bands are calculated at 1581.1, 1594.2 and 1546.0 cm-1 for ligand, Zn-complex and Ni-complex, respectively.

N–N vibrations

The N–N bond stretching vibration at 1065 cm-1 in the experimental spectrum of the ligand is observed in the Zn-complex at 995 cm-1 while these vibrations are recorded at 944 cm-1 in the spectrum of Ni-complex which is a lower frequency region. Calculated values are found to be 1073.9, 1017.7 and 975.5 cm-1 for ligand, Zn-complex and Ni-complex, respectively.

Ring vibrations

C-H stretching bands for the heteroaromatic structures such as furans, pyrroles and thiophenes usually take place in between 3100 and 3000 cm-1 as weak bands because of the small dipole moments of these bonds [30,31]. The symmetric/asymmetric C–H stretching frequencies of thiophene rings are calculated with B3LYP at 3100.8/3083.6 cm-1 for

ligand, at 3112.3/3089.6 cm-1 for Zn-complex and 3120.0/3089.6 cm-1 for Ni-complex. The stretching vibrations of the thiophene ring are generally observed within 1500-1540, 1400-1445 and 1335-1365 cm-1 wavenumber ranges [32,33]. For all complexes, detailed calculation results regarding the stretching vibrations for the thiophene ring are presented in Table 3.

**Table 3.** Comparison of the observed and calculated vibrational frequencies ($cm^{-1}$) for all complexes.

| | B3LYP/6-31G (d,p) | | |
|---|---|---|---|
| Modes | Ligand | Zn-complex | Ni-complex |
| $\nu_{as}NH_2$ | 3298.0 | 3321.6 | 3398.9 |
| $\nu_{s}NH_2$ | 3244.4 | 3274.0 | 3358.8 |
| $\nu$NH | 3186.6 | 3131.0 | - |
| $\nu_{s}CH_{ring}$ | 3100.8 | 3112.3 | 3120.0 |
| $\nu_{as}CH_{ring}$ | 3083.6 | 3089.6 | 3107.1 |
| $\nu_{as}CH_3$ | 3005.5 | 3049.6 | 3001.8 |
| $\nu_{s}CH_3$ | 2919.7 | 2945.0 | 2936.9 |
| $\nu$C=N | 1581.1 | 1594.2 | 1546.0 |
| $\alpha NH_2$ | 1562.1 | 1566.3 | 1577.6 |
| $\nu_{as}C{=}C_{ring}$ | 1533.9 | 1519.9 | 1509.3 |
| $\nu$C=N | - | - | 1495.6 |
| $\gamma$N2H | 1505.3 | 1538.3 | - |
| $\nu_{s}C{=}C_{ring}$ | 1431.2 | 1443.6 | 1413.2 |
| $um CH_3$ | 1366.3 | 1365.5 | 1326.4 |
| $\nu CC_{ring}$ | 1313.6 | 1314.2 | 1304.3 |
| $\beta_{s}CH_{ring}$ | 1197.8 | 1198.3 | 1201.9 |
| $\beta_{as}CH_{ring}$ | 1060.9 | 1044.2 | 1075.7 |
| $\nu$NN | 1073.9 | 1017.7 | 975.5 |
| $\Gamma_{as}CH_{ring}$ | 851.4 | 858.7 | 864.7 |
| $\nu$C=S | 823.3 | 803.8 | - |
| $\Gamma_{s}CH_{ring}$ | 768.9 | 774.5 | 775.4 |
| $\nu$ZnS | | 522.2 | |
| $\nu_{s}$NiS | | | 524.0 |
| $\nu_{s}$NiN | | | 429.6 |
| **RMSE** | 14.74 | 20.09 | 19.40 |

Vibrational modes: ν–stretching, α-scissoring, γ–bending, β–in-plane bending, Γ–out-of–plane, um-umbrella. Subscripts; s: symmetric, as: asymmetric.

### 3.4. Hirshfeld Surface analysis for ligand, Zn- and Ni-complexes

The three-dimensional HSs are generated for the aforementioned structures, and are represented in Figures 3a-c showing surfaces that have been mapped with dnorm (-0.100 to 2.500), shape index (-1.000 to 1.000) and curvedness. As shown in Figure 3a, the Hirshfeld surface for ligand exhibits two bright-red spots near the terminal N–H and S atoms corresponding to donor and acceptor atoms, respectively, which are evidence of the presence of intermolecular N–H···S interactions. The pairwise Cl···S interactions are mapped by faint-red spots that appear on the right and left of the surface. Shape index and curvedness can be used to indicate the presence of stacking arrangements, such as C–H···π and π···π interactions. The shape-index surface indicates a blue convexity representing the donor atom and a red concavity representing the acceptor atom. The large flat region delineated by a blue outline on the curvedness maps refers to the stacking interactions between neighboring molecules. The existence of π···π interactions in the crystal structure of ligand is indicated through the appearance of a flat region around both sides of the thiophene ring in the curvedness plots (Figure 3c),

as well as by red and blue triangles on the thiophene rings in shape-index surface (Figure 3b). Both Cl atoms act as an acceptor to two hydrogen atoms belonging to each of NH2 moieties, separately, and correspond to N–H···Cl bonds which appear as two pairs of darkest-red spots near the Cl-atoms on the Hirshfeld surfaces of Zn-complex. While two of them are shown in Figure 3a, the others are located on the reverse side of the surface. It should be noted that two bright red spots near the NH2 group are also related to the interaction of N–H···Cl. S···Cl/ Cl···S contacts are due to the presence of S···Cl interatomic distances which are shorter than the sum of their van der Waals radii (rvdW: 3.55 Å [34]), and are represented by small, pale-red spots near atoms S and Cl in Figure 3a. In the views of the Hirshfeld surfaces for the Ni-complex in Figure 3a, the bright-red spots near S (thiolate) and the N (imino) atoms reflect intermolecular N–H···S and N–H···N interactions which play a significant role in the formation of inversion dimmers. The presence of a short interatomic H···H, S···H and Cl···S contacts are observable as diminutive, pale-red spots near the thiophene-H and thiophene-H, thiophene-S and methyl-H, as well as thiophene-S and Cl atoms, respectively. The lack of the red and blue triangles on the shape index surface of Zn- and Ni- complexes indicates the absence of stacking interactions, i.e., C–H···π and π···π (Figure 3b). This result has been confirmed by the Hirshfeld surface mapped with curvedness (Figure 3c) and X-ray crystal structural analysis for both complexes [15,18].

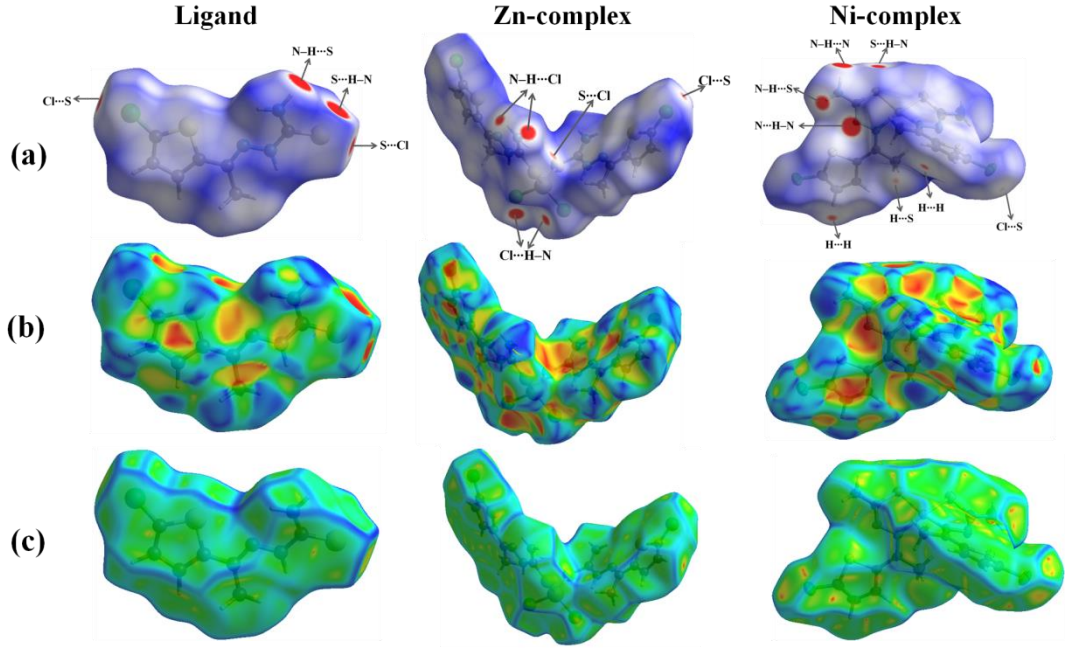


**Figure 3.** View of the Hirshfeld surfaces mapped with (a) ~~d norm~~ $d_{norm}$ with the red spot showing the involvement of the hydrogen bonds and close contacts, (b) shape-index, (c) curvedness for ligand, Zn- and Ni-complexes.

### 3.5. Two-dimensional fingerprint of all complexes

The overall two-dimensional fingerprint plots of all compounds are shown in Figure 4a and those delineated into S···H/H···S, H···H, Cl···H/H···Cl, N···H/H···N, C···C, C···H/H···C, and inter-contacts are illustrated in Figures 4b–g. As expected, Hirshfeld surface analysis of ligand shows that the proportion of S···H/H···S interactions have the greatest contribution (27.1%) to the total Hirshfeld surface, arising from the intermolecular N–HN···S hydrogen-bond linking the two independent molecules. S···H/H···S interactions are viewed as two thin spikes of almost equal lengths at de+ di~2.44 Å in Figure 4b. The next most significant contribution with 23.8% of the overall surface is due to H···H contacts, which indicates van der Waals interactions, and appear as

widely scattered points in the fingerprint maps with the tip at de+ di~2.6 Å (Figure 4c). The FP plots corresponding to Cl···H/H···Cl contacts for ligand have the smallest contribution to the Hirshfeld surface, i.e. 16.4%, compared to Zn- and Ni-complexes, and are reflected in Figure 4d as a symmetrical distribution of points with the edges at de+ di~2.94 Å. C···C contacts only cover about 4.8% of the Hirshfeld surface but are significant due to providing evidence of the π···π interactions which were reported in X-ray diffraction studies. As seen in Figure 4f, C···C contacts appear as points with a rocket-shaped distribution at around de=di~1.8 Å. The absence of characteristic wings in the fingerprint plot as illustrated in Figure 4g, and the smaller percentage of C···H/C···H (6.6%) interactions exhibit inadequate presence of C–H···π interactions in the crystal. This observation also supports X-ray study of the ligand.

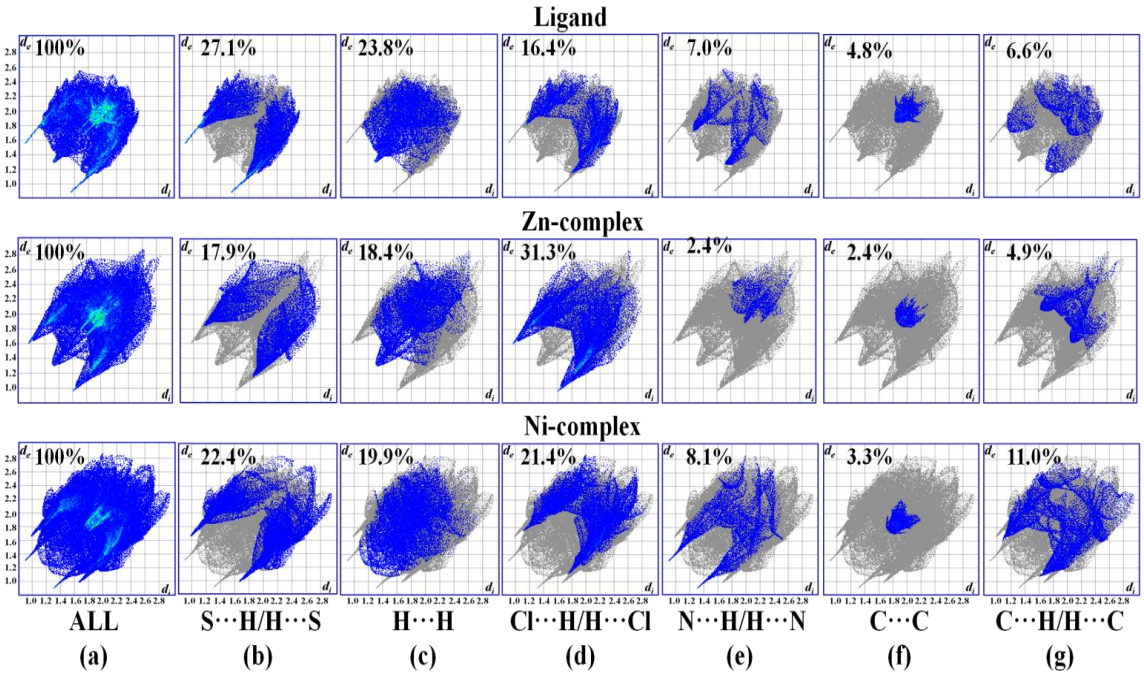


**Figure 4.** Decomposed fingerprint plots along with related HS areas and percentage contributions to the total HS for major intermolecular contacts (a) all (b) S•••H/H•••S, (c) H•••H, (d) Cl•••H/H•••Cl, (e) N•••H/H•••N (f) C•••C and (g) C•••H/H•••C for the all complexes.

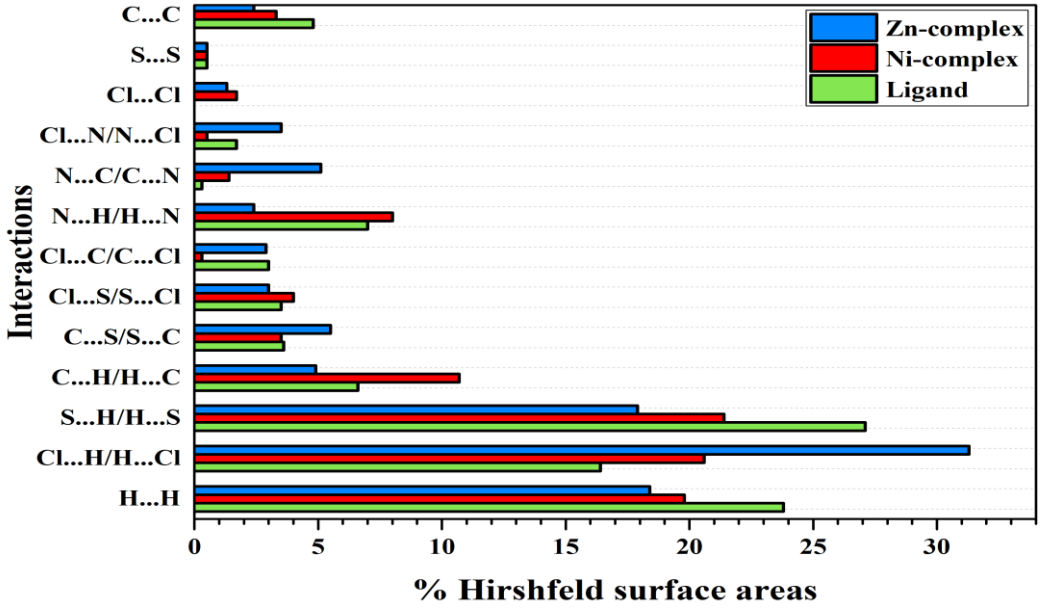

**Figure 5.** Relative contributions to the Hirshfeld surface area for the various intermolecular contacts in all complexes.

Hirshfeld surface analysis of Zn-complex shows an increased amount of Cl···H and H···Cl interactions compared to the ligand and Ni-complex due to the existence of the intermolecular N–H···Cl interactions in the crystal packing. Cl···H/H···Cl contacts which have 31.3 % contribution to the total Hirshfeld surface manifest themselves as two distinct spikes with de+ di~2.3 Å in the 2D fingerprint plots (Figure 4d). The non-directional H···H contacts represent the second important contribution, amounting to 18.4% with a single broad peak at de=di~1.3 Å (Figure 4c). The S···H/H···S interactions, which are indicated by a symmetrical distribution of points with the edges at de+ di~2.98 Å, have the lowest proportion for all of the compounds studied, making up only 17.9% of the overall Hirshfeld surface (Figure 4b). There is a minor contribution of 4.9% to the surface due to C···H/C···H contacts originating from medium or longer contacts in the structure rather than the shorter ones or C–H···π interactions (Figure 4g).

The presence of intermolecular N–HN···S and N–HN···N interactions in Ni-complex is evident from the FP plots delineated into S···H/H···S and N···H/H···N contacts, and these interactions play a pivotal role in the supramolecular arrangement. The S···H/H···S and N···H/H···N contacts are found to contribute a total of 22.4 and 8.1% to the Hirshfeld surface, respectively, which are reflected in the two sharp and narrow spikes of almost equal lengths with their tips at de+di~2.65 Å and de+di~2.19 Å. The pairwise S···H and N···H contacts are demonstrated in Figures 4b and 4e, respectively. In contrast to Zn-complex, the crystal structure of Ni-complex does not exhibit N–H···Cl interactions as pointed out in our earlier X-ray study [15] but the Cl···H/H···Cl interaction comprises 21.4% of the total Hirshfeld surface due to close contacts. The pairwise Cl···H contacts are characterized by a pair of sharp and short symmetric spikes in the two-dimensional fingerprint maps with a prominent long spike at de+di~2.82 Å (Figure 4d) which is approximately less than the sum of van der Waals radii (2.9 Å) [34]. Another notable contact is H···H interaction which is represented by the largest area of the fingerprint plot with a high concentration in the middle region around de, di distances greater than their corresponding van der Waals separations and the proportion of these interactions cover 19.9% of the whole Hirshfeld surface (Figure 4c). Unlike the related interaction observed for ligand and Zn-complex, there is a pair of characteristic wings (with a prominent spike at de+di~2.69 Å) in the two-dimensional fingerprint maps delineated into C···H/C···H contacts. Furthermore, the C···H/C···H interactions make up to 11.0% of the total HS being greater than those observed in ligand and Zn-complex (Figure 4g). These results suggest the influence of the interatomic short C···H contacts instead of intermolecular C–H···π interactions.

Apart from these above, the presence of the small contributions from other remaining interatomic contacts that have a negligible effect on the crystal packing is observed for all compounds. Figure 5 depicts the percentages of contributions to the overall Hirshfeld surface for all contacts in the related compounds.

## 4. Conclusion

In the present study, by the use of quantum chemical calculations we thoroughly have investigated the molecular geometry, vibrational spectra, HOMO and LUMO energies for thiosemicarbazone ligand and its Zn- and Ni-complexes. The geometrical structure parameters for the three compounds are in good agreement with available related experimental crystal data. In comparison to bond angles, our results indicate that there exists a negligible deviation for bond lengths. The FT-IR vibrational frequencies of all compounds are calculated and the vibrational assignments corresponding to wavenumbers have been determined and compared with their experimental spectrum.

The study of X-ray diffraction and analysis of FT-IR spectra shows unambiguously that the thiosemicarbazone ligand coordinated to Zinc ion remains as a thione tautomer while the ligand coordinated to Ni atom appears as a thiol form. Through the molecular orbital analysis, we found that the energy gap between HOMO and LUMO is

largest for Zn-complex which indicates that Zn-complex is more stable and less reactive than ligand and Ni-complex. Also, analyses of intermolecular interactions and close contacts in the crystal structures of all compounds have been performed by visualizing Hirshfeld surface and 2D fingerprint plots.

**Acknowledgments**

The author thanks Muhittin Aygün from Dokuz Eylül University, Department of Physics for the use of the Gaussian 09W/G View package programs. Dokuz Eylül University for the use of the Oxford Rigaku Xcalibur Eos Diffractometer (purchased under University Research Grant No: 2010.KB.FEN.13) is also greatly acknowledged.

**References**

[1] R.K. Singh, A.K. Singh, Synthesis, molecular structure, spectral analysis, natural bond order and intramolecular interactions of 2-acetylpyridine thiosemicarbazone: a combined DFT and AIM approach. J. Mol.Struct.1094 (2015) 61-72.

[2] K. Alomar, M.A. Khan, M. Allain, G. Bouet, Synthesis, crystal structure, and characterization of 3-thiophene aldehyde thiosemicarbazone and its complexes with cobalt(II), nickel(II) and copper(II). Polyhedron 28 (2009) 1273-1280.

[3] T.S. Lobana, P. Kumari, M. Zeller, R.J. Butcher, The influence of the substituents at N1 nitrogen on geometry of nickel(II) complexes with heterocyclic thiosemicarbazones. Inorg. Chem. Commun. 11 (2008) 972-974.

[4] E. Pahonțu, C. Paraschivescu, D.-C. Ilieș, D. Poirier, C. Oprean, V. Păunescu, A. Gulea, T. Roșu, O. Bratu, Synthesis and Characterization of Novel Cu(II), Pd(II) and Pt(II) Complexes with 8-Ethyl-2-hydroxytricyclo(7.3.1.02,7)tridecan-13 onethiosemicarbazone: Antimicrobial and in Vitro Antiproliferative Activity. Molecules 21 (2016) 674–692.

[5] M.-X. Li, D. Zhang, L.-Z. Zhang, J.-Y. Niu, Synthesis, crystal structures, and biological activities of 2-thiophene N(4)-methylthiosemicarbazone and its unusual hexanuclear silver(I) cluster. Inorg. Chem. Commun. 13 (2010) 1268-1271.

[6] K. Alomar, A. Landreau, M. Kempf, M.A. Khan, M. Allain, G. Bouet, Synthesis, crystal structure, characterization of zinc(II), cadmium(II) complexes with 3-thiophene aldehyde thiosemicarbazone (3TTSCH). Biological activities of 3TTSCH and its complexes. J. Inorg. Biochem. 104 (2010) 397-404.

[7] R.A. Finch, M.C. Liu, S.P. Grill, W.C. Rose, R. Loomis, K.M. Vasquez, Y.C. Cheng, A.C. Sartorelli, Triapine (3-Aminopyridine-2-carboxaldehyde thiosemicarbazone): A Potent Inhibitor of Ribonucleotide Reductase Activity with Broad Spectrum Antitumor Activity. Biochem. Pharmacol. 59 (2000) 983-991.

[8] Z. Tavsan, P.K. Yaman, E. Subasi, H.A. Kayali, Screening organometallic thiophene containing thiosemicarbazone ruthenium (II/III) complexes as potential anti tumour agents. J. Biol. Inorg. Chem. 23 (2018) 425-435.

[9] M. Khandani, T. Sedaghat, N. Erfani, M.R. Haghshenas, H.R. Khavasi, Synthesis, spectroscopic characterization, structural studies and antibacterial and antitumor activities of diorganotin complexes with 3-methoxysalicylaldehyde thiosemicarbazone. J. Mol. Struct. 1037 (2013) 136-143.

[10] N. Öztürk, P. Kose Yaman, M. Yavuz, Ö. Öter, S. Timur, E. Subaşı, Synthesis, structural characterization, oxygen sensitivity, and antimicrobial activity of ruthenium(II) carbonyl complexes with thiosemicarbazones. J. Coordin. Chem. 67 (2014) 2688-2700.

[11] R. Pingaew, S. Prachayasittikul, S. Ruchirawat, Synthesis, Cytotoxic and Antimalarial Activities of Benzoyl Thiosemicarbazone Analogs of Isoquinoline and Related Compounds. Molecules 15 (2010) 988-996.

[12] P. Chellan, S. Nasser, L. Vivas, K.G.S. Smith, Cyclopalladated complexes containing tridentate thiosemicarbazone ligands of biological significance: Synthesis, structure and antimalarial activity. J. Organomet. Chem. 695 (2010) 2225-2232.

[13] S. Sharma, F. Athar, M. R. Maurya, A. Azam, Copper(II) complexes with substituted thiosemicarbazones of thiophene-2-carboxaldehyde: synthesis, characterization and

antiamoebic activity against E. Histolytica. Eur. J. Med. Chem. 40 (2005) 1414-1419.

[14] N. Gokhale, S. Jain, M. Yadav, Design and Virtual Screening Towards Synthesis of Novel Substituted Thiosemicarbozones as Ribonuleotide Reductase (RNR) Inhibitors with Improved Cellular Trafficking and Anticancer Activity. Curr. Top. Med. Chem. 15 (2015) 37-42.

[15] B. Şen, H. K. Kalhan, V. Demir, E.E. Güler, H. Ayar Kayali, E. Subaşı, Crystal structures, spectroscopic properties of new cobalt(II), nickel(II), zinc (II) and palladium(II) complexes derived from 2-acetyl-5-chloro thiophene thiosemicarbazone: Anticancer evaluation Mater. Sci. Eng. C 98 (2019) 550-559.

[16] D.K. Demertzi, A. Domopoulou, M.A. Demertzis, G. Valle, A. Papageorgiou, Palladium(II) complexes of 2-acetylpyridine N(4)-methyl, N(4)-ethyl and N(4)-phenyl-thiosemicarbazones. Crystal structure of chloro(2-acetylpyridine N(4)-methylthiosemicarbazonato) palladium(II). Synthesis, spectral studies, in vitro and in vivo antitumour activity. J. Inorg. Biochem. 68 (1997) 147–155.

[17] Y. Tian, C. Duan, C. Zhao, X. You, T.C.W. Mak, Z.Y. Zhang, Synthesis, Crystal Structure, and Second-Order Optical Nonlinearity of Bis(2-chlorobenzaldehyde thiosemicarbazone)cadmium Halides (CdL2X2; X ) Br, I). Inorg. Chem. 36 (1997) 1247-1252.

[18] P. Kose Yaman, B. Şen, C.S. Karagoz, E. Subaşı, Half-sandwich ruthenium-arene complexes with thiophen containing thiosemicarbazones: Synthesis and structural characterization. J. Organomet. Chem. 832 (2017) 27-35.

[19] A.D. Becke, Density-functional thermochemistry. III. The role of exact exchange. J. Chem. Phys. 98 (1993) 5648.

[20] C. Lee, W. Yang, R.G. Parr, Development of the Colle-Salvetti correlation-energy formula into a functional of the electron density. Phys. Rev. B Condens. Matter 37 (1988) 785.

[21] A.D. McLean, G.S. Chandler, Contracted Gaussian basis sets for molecular calculations. I. Second row atoms, Z=11–18. J. Chem. Phys. 72 (1980) 5639.

[22] M.J. Frisch, G.W. Trucks, H.B. Schlegel, G.E. Scuseria, M.A. Robb, J.R. Cheeseman, G. Scalmani, V. Barone, B. Mennucci, G.A. Petersson, H. Nakatsuji, M. Caricato, X. Li, H.P. Hratchian, A.F. Izmaylov, J. Bloino, G. Zheng, J.L. Sonnenberg, M. Hada, M. Ehara, K. Toyota, R. Fukuda, J. Hasegawa, M. Ishida, T. Nakajima, Y. Honda, O. Kitao, H. Nakai, T. Vreven, J.A. Montgomery Jr., J.E. Peralta, F. Ogliaro, M. Bearpark, J.J. Heyd, E. Brothers, K.N. Kudin, V.N. Staroverov, T. Keith, R. Kobayashi, J. Normand, K. Raghavachari, A. Rendell, J.C. Burant, S.S. Iyengar, J. Tomasi, M. Cossi, N. Rega, J.M. Millam, M. Klene, J.E. Knox, J.B. Cross, V. Bakken, C. Adamo, J. Jaramillo, R. Gomperts, R.E. Stratmann, O. Yazyev, A.J. Austin, R. Cammi, C. Pomelli, J.W. Ochterski, R.L. Martin, K. Morokuma, V.G. Zakrzewski, G.A. Voth, P. Salvador, J.J. Dannenberg, S. Dapprich, A.D. Daniels, O. Farkas, J.B. Foresman, J.V. Ortiz, J. Cioslowski, D.J. Fox, Gaussian 09, Revision D.01, Gaussian Inc., Wallingford, CT, 2013.

[23] A. Frisch, H.P. Hratchian, R.D. Dennington, II, T.A. Keith, John Millam, B. Nielsen, A.J. Holder, J. Hiscocks, GaussView Version 5.0.8, Gaussian Inc, Wallingford, CT, USA, 2009.

[24] F.L. Hirshfeld, Bonded-atom fragments for describing molecular charge densities. Theor. Chim. Acta 44 (1977) 129-138.

[25] S.K. Wolff, D.J. Grimwood, J.J. McKinnon, M.J. Turner, D. Jayatilaka, M.A. Spackman, CrystalExplorer 3.1 (2013), University of Western Australia, Crawley, Western Australia, 2005-2013,
http://hirshfeldsurface.net/CrystalExplorer.

[26] M.A. Palafox, DFT computations on vibrational spectra: Scaling procedures to improve the wavenumbers. Phys. Sci. Rev. 3 (2018) 1-30.

[27] M. Szafran, A. Katrusiak, J. Koput, Z. Dega-Szafran, X-ray, MP2 and DFT studies of the structure, vibrational and NMR spectra of homarine. J. Mol. Struct.846 (2007) 1-12.

[28] J.A. Pople, H.B. Schlegel, R. Krishnan, D.J. Defrees, J.S. Binkley, M.J. Frisch, R.A. Whiteside, R.F. Hout. W.J. Hehre, Molecular orbital studies of vibrational frequencies. Int. J. Quantum Chem. 15 (1981) 269-278.

[29] M. Silverstein, G.C. Basseler, C. Morill, Spectrometric Identification of Organic Compounds, Wiley, New York, 1981.

[30] C.N.R. Rao, Chemical Application of Infrared Spectroscopy , Academic Press, New york,1981.

[31] N. Sundaraganesan, H. Saleem, S. Mohan, Spectrochimica Acta Part A, Vibrational spectra, assignments and normal coordinate analysis of 3-aminobenzyl alcohol. 59 (2003) 2511- 2517.

[32] S.Ya. Khorshev, N.S. Vyazankin, A.N. Egorochkin, E.A. Chernyshev, V.I. Savushkina, O.V. Kuz'min, V.Z. Anisimova, Spectroscopic study of organosilicon derivatives of thiophene. Chemistry of Heterocyclic Compounds, 10 (1974) 413–417.

[33] Socrates, Infrared and Raman Characteristic Group Frequencies, Tables and Charts, Wiley, New York, 1974.

[34] A. Bondi, van der Waals Volumes and Radii. J.Phys.Chem. 68 (1964) 441-451.